

## Semiconductive Polymer Blends: Correlating Structure with Transport Properties at the Nanoscale\*\*

By Cristian Ionescu-Zanetti, Adam Mechler,  
Sue A. Carter, and Ratnesh Lal\*

Conjugated polymer blends are the focus of scientific and commercial interest due to their wide range of applications, from organic light-emitting diodes (LEDs)<sup>[1]</sup> and organic polymer electronics<sup>[2]</sup> to chemical sensors,<sup>[3]</sup> biological sensors,<sup>[4]</sup> and microactuators.<sup>[5]</sup> Poly(3,4-ethylenedioxythiophene) (PEDOT) is a semiconducting polymer that becomes conductive when doped with either poly(styrene sulfonate) (PSS) or other charged groups, such as  $\text{PF}_6^-$ . PEDOT-PSS is a member of a class of polymers used as charge-injecting electrodes. In particular, it holds promise for applications such as polymer LEDs<sup>[1]</sup> and solar cells.<sup>[6]</sup> For electro-optical devices such as LEDs and solar cells, improving efficiency requires a detailed understanding of the molecular superstructure of the blend and control of transport properties.<sup>[7]</sup> The role of interfaces (e.g., indium tin oxide (ITO)-polymer) in injection efficiency was recently highlighted,<sup>[8]</sup> and previous scanning tunneling microscopy (STM) studies suggest that the polymer morphological inhomogeneities strongly influence the charge carrier injection and transport properties.<sup>[9]</sup>

For structural studies, macroscopic methods such as X-ray diffraction (XRD) are often employed.<sup>[10]</sup> These methods average over a large area, typically over  $1 \text{ mm}^2$ , giving a view of the overall structural properties. The paracrystalline structure of tosylate doped PEDOT blends was shown by XRD.<sup>[10]</sup> Anisotropies in sample conductivity have been determined by bulk methods,<sup>[11]</sup> and comparison with X-ray data demonstrates that the orientation of the lamellae shows a clear correlation with the conductivity-anisotropy. In particular, conductivity is higher parallel to the plane of lamellar orientation. There is a lack of information, however, about the local morphology of the blend, as well as about the effect of structural features on charge injection at the polymer surface.

Atomic force microscopy (AFM) is a widely used surface characterization tool. In addition to morphological characterization, AFM also has spectroscopic capabilities. Phase imaging AFM (PI-AFM) is sensitive to the nature of the tip-surface interaction, and therefore to the material composition.<sup>[12]</sup> In addition, when combined with the new high-sensitivity conductive working mode (C-AFM),<sup>[13]</sup> local structural, compositional, and transfer properties can be studied on a nanometer scale. Unlike transmission electron microscopy (TEM) measurements,<sup>[14]</sup> C-AFM allows imaging morphology in parallel with local currents. Recording such a multi-dimensional map assures that matching sets of the different sample properties are collected.

In the present study we apply multimodal AFM to map the local charge transfer properties in correlation to the molecular superstructure of the polymer blend. We identify the structural basis of the correlation between charge injection efficiency and local blend composition. At the polymer surface, our results show that efficient charge injection occurs in regions where the lamellar edges are exposed to the probe. This correlation suggests that the efficiency of charge injection at the polymer-electrode interface can be enhanced by controlling lamellar orientation.

Large-scale scanning electron microscopy (SEM) imaging of the PEDOT-PSS surface (Fig. 1) reveals an anisotropic surface, in terms of metallic properties. Electron-rich regions vary in size from  $5\text{--}30 \mu\text{m}$  (bright regions, Fig. 1). The PEDOT-PSS blend has an average thickness of  $1 \mu\text{m}$  (marked A on the SEM

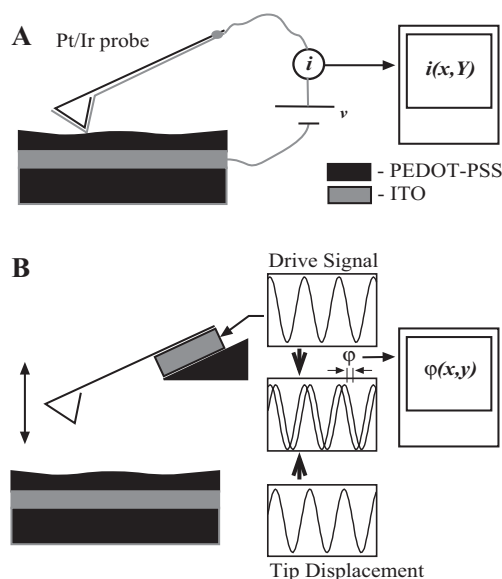


**Figure 1.** A schematic representation of the AFM imaging modes employed. A) In C-AFM, a conductive tip is biased with respect to the sample at a voltage  $V$ . Current measurements are taken while the tip raster scans the surface and assembled into a map of current intensity. B) Phase images (PI-AFM) are obtained in tapping mode AFM. The phase shift between the piezo drive signal and the cantilever oscillation is measured at each point and assembled into a phase image of the surface.

[\*] Prof. R. Lal, Dr. C. Ionescu-Zanetti, Dr. A. Mechler<sup>[†]</sup>  
Neuroscience Research Institute, University of California  
Santa Barbara, CA 93106 (USA)  
E-mail: lal@lifesci.ucsb.edu

Dr. S. A. Carter  
Physics Department, University of California  
Santa Cruz, CA 95064 (USA)

[†] Dr. A. Mechler is on leave from the Research Group on Laser Physics of the Hungarian Academy of Sciences, Szeged, Hungary 6701.

[\*\*] The authors thank M. Lefevre, R. Puestow, and P. Harris of Digital Instruments for access to conductive AFM hardware. We also thank Luisa Bozano and Campbell Scott (IBM Almaden) for helpful discussions. This work was supported by Phillip Morris External Grant Program and NIH (CIZ, RL), NSF-NATO (AM, RL), BIOSTAR-UC-ABT Inc. (CIZ, RL) NSF grant ECS0101794 (SAC).

image of the cross-section, Fig. 2 inset), while the bottom ITO electrode (arrow, Fig. 2 inset) is 200 nm thick.

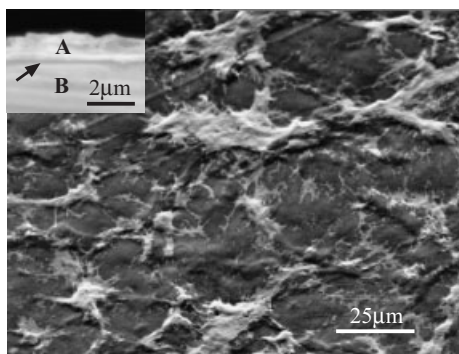


**Figure 2.** Scanning electron micrographs of the PEDOT-PSS film in cross-section (inset) and top view. In the cross-section, the horizontal band labeled A is the PEDOT-PSS layer, while an arrow indicates the thin band that is the ITO bottom electrode on top of the insulating plastic substrate (labeled B).

The AFM experimental setup used is shown in Figure 2. Height mode images of PEDOT-PSS show two types of distinct surface structures, a rough one and a smooth one (Fig. 3A). They can be unambiguously distinguished in the first derivative of the height image (Fig. 3B), which highlights sharp features (edges).

The corresponding current map is obtained by biasing the conductive tip (Pt/Ir coated Si tip) at a constant voltage with respect to the ITO substrate and recording current intensities at each image pixel (C-AFM, Fig. 2A). C-AFM measurements (Fig. 3C) reveal an average current of 10 pA at a bias of 6 V recorded over rough regions, while on the smooth regions of the sample the current is below instrument sensitivity.

Phase data for the same sample area was obtained in tapping mode AFM (TM-AFM, Fig. 2B).<sup>[15]</sup> Phase imaging has previously been used to visualize different chemical components of nanostructured surfaces.<sup>[12]</sup> PI-AFM was used to map the local physical properties of the sample along with the morphology. Phase images of the conductive regions reveal significantly higher phase shift variability as compared to the insulating regions (Fig. 3D). An overlay of conductivity data (from Fig. 3C) onto a three-dimensional (3D) representation of topography (from Fig. 3A) is presented in Figure 3E. Current is represented by the color scale (0–60 pA).

In order to elucidate the differences between the conductive and insulating regions of Figure 3E, we imaged the interface between the two regions (small square in Fig. 3E). The height and phase mode images of the  $450 \times 450 \text{ nm}^2$  area are shown in Figures 3F,G. While the lower part of Figure 3F (area 2) is flat, the upper part shows a number of sharp edges and corrugated features (area 1). The phase image of area 1 (Fig. 3G) shows numerous sharp phase changes ( $\sim 25^\circ$ ), which are not present in area 2 of the image. The phase changes appear in proximity to edges seen in Figure 3F. Thus, higher con-

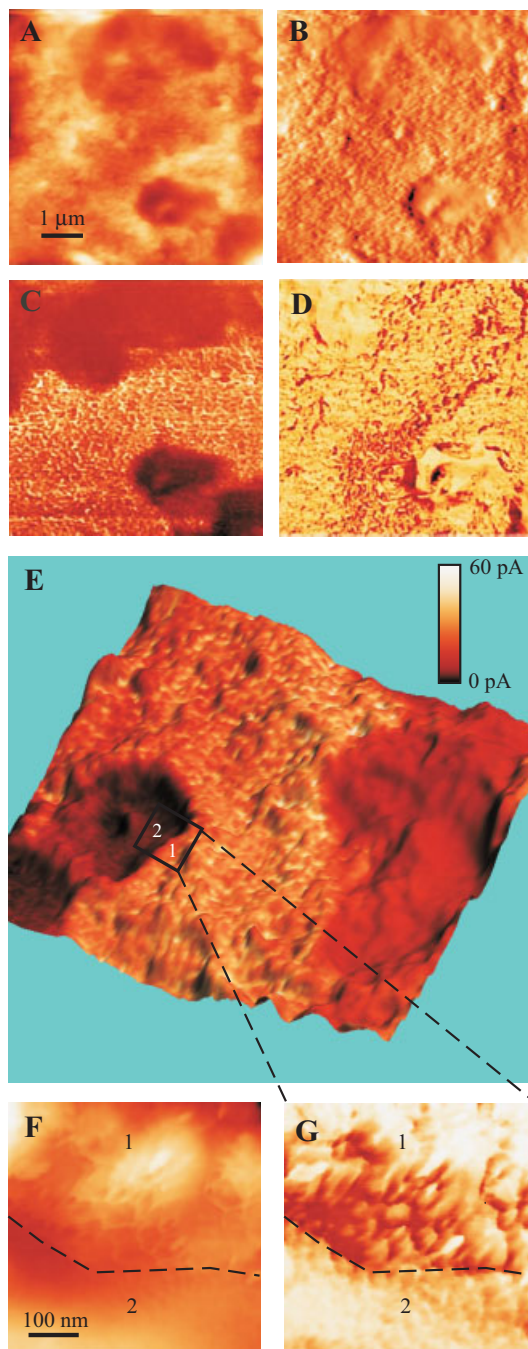


**Figure 3.** Atomic force microscope images of A) topography, B) the first derivative of topography, C) conductivity, and D) phase of a thin PEDOT-PSS film. Highly conductive regions are co-localized with regions of high roughness and high phase variability. In contrast, the conductivity of flat regions is lower by at least two orders of magnitude. e) A 3D overlay of current and topography. The color scale represents current (0–60 pA) and is projected onto the 3D representation of the height data from (A). F) A topography zoom into the interface region marked by a square on (E); G) is the corresponding phase image. Panel (F) (height) shows a smooth region (2) and a rougher lamellar region (1). The height scale ranges from 0–56 nm (dark–light). The phase scale is from 0–70°.

ductivity is a feature of regions where the sample topography contains a large number of edges and high phase variability.

Higher resolution (smaller scan size) images of the region of the sample that showed high conductivity are presented in Figure 4. At this scale, the terraced structure of the polymer surface becomes evident. The surface morphology suggests that the polymer is organized into lamellar building blocks of an approximate thickness of 3 nm (Fig. 4A–C). By comparison, X-ray measurements of PEDOT doped with thiosilicate ions, a smaller dopant, showed a spacing of 1.4 nm between PEDOT lamella.<sup>[10]</sup>

In Figure 4B the phase data has been projected onto the 3D reconstruction of the topography. Note that lamellar edges are often marked by a phase change. Some transitions from one layer to another show only a transient phase shift at the layer step, related to topographic perturbation of the phase.<sup>[12]</sup> In this case, the two layers consist of the same material. Other layer to layer transitions are accompanied by a 25° phase shift, indicating a change in the nature of tip–surface interaction,<sup>[12]</sup> and thus a different material composition of the bottom layer (Fig. 4B,D). Accordingly, the paracrystalline structure of PEDOT–PSS is explained by a layered structure with PSS sandwiched between some of the PEDOT layers (Fig. 4E).

From PEDOT–PSS current maps one can estimate the conductivity perpendicular to the surface. Averaging over all image pixels and assuming a tip–sample contact area of 100 nm<sup>2</sup> yields an average sample conductivity  $\sigma = 2.5 \times 10^{-4} \Omega^{-1} \text{ cm}^{-1}$  normal to the substrate plane. By comparison, our macroscopic in-plane conductivity measurement for the same blend was four orders of magnitude higher ( $5 \Omega^{-1} \text{ cm}^{-1}$ ). This agrees well

with reported in-plane bulk conductivities for PEDOT–PSS blends,<sup>[6]</sup> which are in the range of  $1\text{--}10 \Omega^{-1} \text{ cm}^{-1}$ . For conductivity normal to the substrate plane, no other measurements are available.

Previous studies suggest that charge mobilities are considerably higher along polymer lamellae, as compared to normal mobilities for polymer-based conductors with a transport mechanism similar to PEDOT.<sup>[11]</sup> Our data show that high currents are associated with regions where a high number of lamellar edges are exposed. This implies that in regions where the AFM tip has access to orbitals that belong to a lamellar edge, efficient charge transport occurs. Therefore, high currents are observed. In contrast, when the AFM tip is scanning on top of an intact lamella, the transport is limited by the high inter-sheet barrier.

In order to estimate carrier mobility, current–voltage ( $I$ – $V$ ) characteristics of different parts of the sample can be obtained by varying the bias applied to the AFM tip. The microscopic  $I$ – $V$  curve presented in Figure 5 was obtained at a conductive location on the PEDOT–PSS sample. While macroscopic  $I$ – $V$  curves show ohmic behavior (data not shown), microscopic  $I$ – $V$  curves show a quadratic dependence on the bias. In the microscopic case small tip–sample contact areas ( $\sim 100 \text{ nm}^2$ ) lead to current densities at the point of contact that are on the order of  $10^5 \text{ A m}^{-2}$ . Since macroscopic current densities at the contacts are smaller by about four orders of magnitude, microscopic  $I$ – $V$  measurements probe a regime of very high local current density. The observed quadratic dependence of voltage

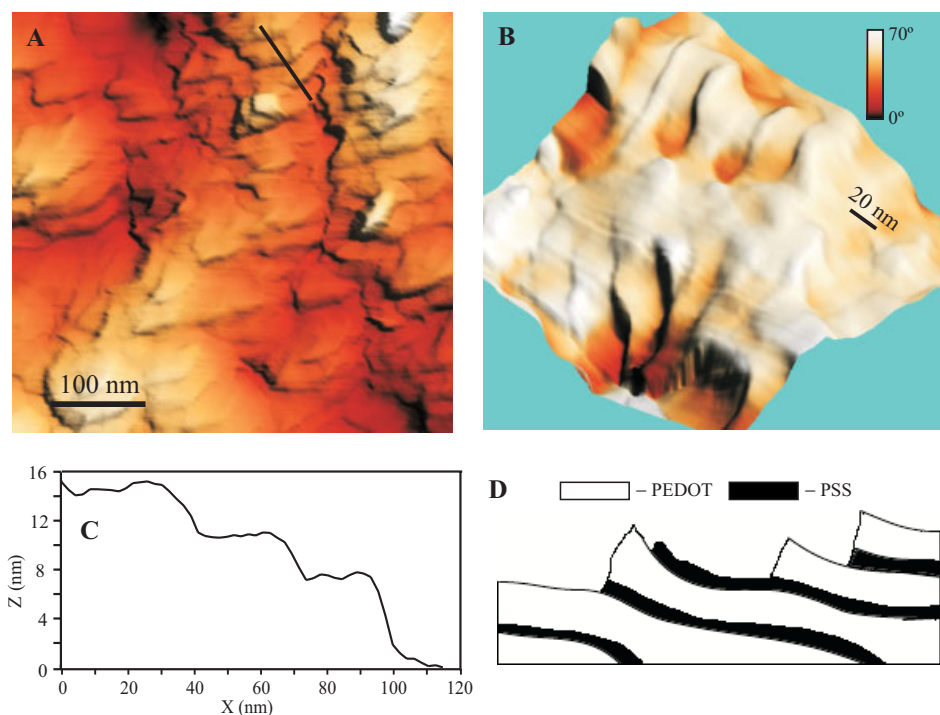


**Figure 4.** A) Detailed structure of a highly conductive region of the sample. B) A 3D overlay of morphology and phase data at higher resolution. The color scale indicates phase shifts and ranges from 0–70°. C) A section profile along the line segment in (B). It shows the edges of several sheets, with an average step height of  $\sim 3$  nm. D) A schematic of the proposed PEDOT–PSS structure.



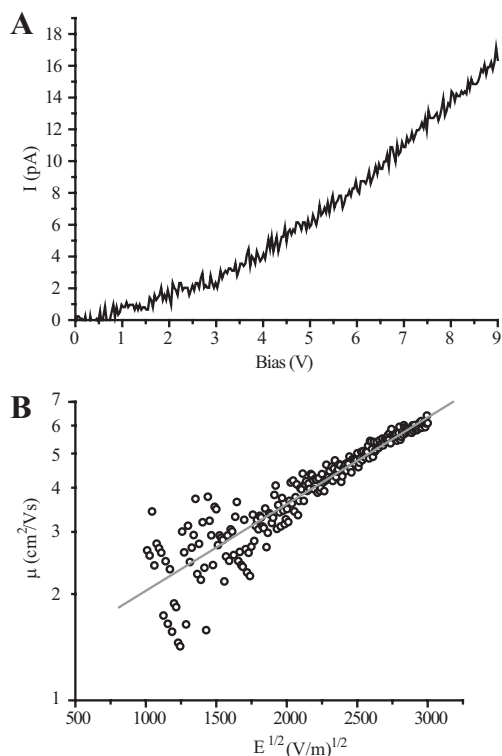


**Figure 5.** a) Current–voltage relation for the tip–sample path over a conductive region of the PEDOT–PSS blend. The bias voltage is applied to the sample with respect to the tip. b) Mobility plotted as a function of  $E$  field. Superimposed on the mobility data is a linear fit, following the predictions of SLSC ( $\mu \propto E^{1/2}$ ).

on current suggests that the junction can be described by space charge limited current models (SCLC), as applied to previous conductive probe experiments.<sup>[16]</sup> The microscopic current density ( $J$ ) fits the simple analytical relation for space charge-limited injection as derived by Mott and Gurney<sup>[17]</sup>

$$J = \frac{9}{8} \mu \epsilon \epsilon_0 \frac{V^2}{L^3} \quad (1)$$

where  $V$  is the bias,  $L$  is the thickness of the material,  $\mu$  is the charge-carrier mobility, and  $\epsilon \epsilon_0$  is the dielectric constant. The hole mobility obeys the Poole–Frankel relationship

$$\mu = \mu_0 e^{\sqrt{E/E_0}} \quad (2)$$

where  $\mu_0$  is the zero-field mobility,  $E$  the electric field, and  $E_0$  the field coefficient. Using Equation 1 with  $E = V/L$ , we may plot the mobility versus the applied field (Fig. 4B). The straight line fit corresponds to Equation 2. The fit parameters are  $\mu_0 = 0.065 \pm 0.015$  and  $\sqrt{E_0} = 2.5 \times 10^{-5}$ . This gives an estimate for  $\mu_0$  and  $E_0$  for the PEDOT–PSS film in a direction perpendicular to the substrate.

In summary, we present a high-resolution morphology, conductivity and phase-shift AFM study of a conductive polymer blend, PSS-doped PEDOT. PEDOT–PSS has a paracrystalline structure that consists of molecular lamellae of PEDOT

and PSS. The interlamellar distance was estimated to be 3 nm by AFM. Efficient charge injection occurs in regions where the AFM tip can contact orbitals from exposed PEDOT lamellar edges. When probing the top lamella, low currents are observed. Accordingly, transport largely occurs along the lamellae, leading to anisotropic injection efficiency along the top surface and the increased conductivity in the  $xy$  plane that has been observed by bulk methods. The distribution of the two different blend components is visualized by phase-imaging AFM. This correlation offers insight into the structural underpinnings of charge transport and can be applied to a variety of conductive polymer blends. Our results suggest that injection efficiency for macroscopic contacts to PEDOT–PSS surfaces can be improved by controlling lamellar orientation at the polymer–metal interface.

### Experimental

**Sample Preparation:** PEDOT–PSS (Agfa, Orgacon) [18] was solution cast on a plastic–ITO substrate and annealed for 1 h at 100 °C. The resulting polymer layer is 1  $\mu\text{m}$  thick, while the bottom ITO layer is 200 nm thick (Fig. 2 inset).

**Atomic Force Microscopy:** Electrical current was measured with the AFM tip in continuous contact with the surface (contact-mode AFM—see Fig. 1A). A conductive tip (Pt/Ir coated Si tip) is biased at a constant voltage with respect to the indium tin oxide (ITO) substrate. Current intensities are recorded at each image pixel while the AFM tip raster scans the surface (Fig. 1A).

Phase data for the same sample area was obtained by tapping-mode AFM (TM-AFM) [15]. In this working mode the cantilever is driven at its resonance frequency via a piezoelectric actuator and the amplitude and phase of oscillation is monitored (see Fig. 1B). When this oscillating probe is moved into the non-linear force field of the surface, the amplitude decreases while the phase lag between the drive and the measured signal changes as a function of the tip–surface interaction. The amplitude is maintained at a constant value by controlling the probe–surface distance during scanning, such that it is tracking the surface morphology. The phase shift map is recorded simultaneously by phase-imaging-mode AFM, PI-AFM [19].

Received: July 25, 2003  
Final version: October 30, 2003

- [1] S. A. Carter, M. Angelopoulos, S. Karg, P. J. Brock, J. C. Scott, *Appl. Phys. Lett.* **1997**, *70*, 2067.
- [2] B. Crone, A. Dodabalapur, Y. Y. Lin, R. W. Filas, Z. Bao, A. LaDuca, R. Sarpeshkar, H. E. Katz, W. Lin, *Nature* **2000**, *403*, 521.
- [3] C. Hagleitner, A. Hierlemann, D. Lange, A. Kummer, N. Kerness, O. Brand, H. Baltes, *Nature* **2001**, *414*, 293.
- [4] G. Chen, Z. Guan, C. T. Chen, L. Fu, V. Sundaresan, F. H. Arnold, *Nat. Biotechnol.* **1997**, *15*, 354.
- [5] E. W. H. Jager, E. Smela, O. Inganas, *Science* **2000**, *290*, 1540.
- [6] L. B. Groenendaal, F. Jonas, D. Freitag, H. Pielartzik, J. R. Reynolds, *Adv. Mater.* **2000**, *12*, 481.
- [7] P. K. H. Ho, J.-S. Kim, J. H. Burroughes, H. Becker, S. F. Y. Li, T. M. Brown, F. Cacialli, R. H. Friend, *Nature* **2000**, *404*, 481.
- [8] J. Cui, Q. L. Huang, J. C. G. Veinot, H. Yan, Q. W. Wang, G. R. Hutchison, A. G. Richter, G. Evmnenko, P. Dutta, T. J. Marks, *Langmuir* **2002**, *18*, 9958.
- [9] S. F. Alvarado, S. Barth, H. Bussler, U. Scherf, J. W. van der Horst, P. A. Bobbert, M. A. J. Michels, *Adv. Funct. Mater.* **2002**, *12*, 117.

- [10] K. E. Aasmundtveit, E. J. Samuelsen, L. A. A. Pettersson, O. Inganas, T. Johansson, R. Feidenhans'l, *Synth. Met.* **1999**, *101*, 561.
- [11] H. Sirringhaus, P. J. Brown, R. H. Friend, M. M. Nielsen, K. Bechgaard, B. M. W. Langeveld-Voss, A. J. H. Spiering, R. A. J. Janssen, E. W. Meijer, P. Herwig, D. M. de Leeuw, *Nature* **1999**, *401*, 685.
- [12] a) A. Mechler, J. Kokavecz, P. Heszler, R. Lal, *Phys. Rev. Lett.* **2003**, *82*, 3740. b) N. A. Burnham, O. P. Behrend, F. Oulevey, G. Gremaudi, P. J. Gallo, D. Gourdon, E. Dupas, A. J. Kulik, H. M. Pollock, G. A. D. Briggs, *Nanotechnology* **1997**, *8*, 67.
- [13] a) C. Ionescu-Zanetti, K. Cheung, R. Lal, L. P. Lee, *J. Appl. Phys.* **2003**, *93*, 10134. b) F. Houze, R. Meyer, O. Schneegans, L. Boyer, *Appl. Phys. Lett.* **1996**, *69*, 1975.
- [14] D. Fichou, F. Charra, A. O. Gusev, *Adv. Mater.* **2001**, *13*, 555.
- [15] a) R. Lal, S. A. John, *Am. J. Physiol.* **1994**, *266*, C1. b) C. Ionescu-Zanetti, R. Khurana, J. R. Gillespie, J. S. Petrick, L. C. Trabachino, L. J. Minert, S. A. Carter, A. L. Fink, *Proc. Natl. Acad. Sci. USA* **1999**, *96*, 13175.
- [16] H. N. Lin, H. L. Lin, S. S. Wang, L. S. Yu, G. Y. Perng, S. A. Chen, S. H. Chen, *Appl. Phys. Lett.* **2002**, *81*, 2572.
- [17] N. F. Mott, R. W. Gurney, *Electronic Processes in Ionic Crystals*, Oxford University Press, London **1948**.
- [18] [http://www.agfa.com/sfc/pdf/OrgaconPasteTransparent\\_datasheet.pdf](http://www.agfa.com/sfc/pdf/OrgaconPasteTransparent_datasheet.pdf)
- [19] G. Friedbacher, H. Fuchs, *Pure Appl. Chem.* **1999**, *71*, 1337.

## Polyelectrolyte Micropatterning Using a Laminar-Flow Microfluidic Device\*\*

By Dmitry G. Shchukin, Dinesh S. Kommireddy, Yongjun Zhao, Tianhong Cui, Gleb B. Sukhorukov, and Yuri M. Lvov\*

The study of inter-polyelectrolyte complex formation at interfaces is one of the important areas of interfacial and polymer chemistry. Linear polyelectrolyte,<sup>[1]</sup> DNA/polyelectrolyte,<sup>[2]</sup> and protein/polyelectrolyte<sup>[3]</sup> systems have been studied in bulk solution. Protective, synergetic, catalytic, and hydrophilic (hydrophobic) effects of polyelectrolyte/biomacromolecule combinations could be demonstrated. Such composite polyelectrolyte structures are of practical importance for medical purposes, as components of biosensors, protective coatings, and as biocompatible tools for targeted DNA or enzyme delivery in cells. A number of approaches, including layer-by-layer assembly,<sup>[4]</sup> mixing of polyelectrolytes in stoichiometric and non-stoichiometric ratios,<sup>[1]</sup> and in-situ inter-

polymerization<sup>[5]</sup> have been developed to provide polyelectrolyte structures with desired composition, properties, and biofunctionality. Ordered, functional polyelectrolyte microstructures allow the production of nanoengineered systems for cell treatment and complex inter-polyelectrolyte sensor elements.<sup>[6]</sup> Conventional photolithography was used to fabricate such microstructures;<sup>[7]</sup> however it is not applicable for biological materials, because in photolithographic processes high-energy physical or aggressive chemical treatments are required. Therefore, lithographic methods have strong limitations with respect to the type of materials that can be employed and the resulting microstructures.

One of the most facile and versatile approaches for microfabrication in mild, ambient conditions is laminar-flow synthesis inside microchannels, as proposed by Whitesides and co-workers.<sup>[8]</sup> This method employs a laminar stream of two or more miscible solutions in one capillary or microchannel. Laminar streams of multiple solutions in the same channel flow individually, and the only method of interaction between dissolved reagents is transverse molecular diffusion. A multiphase laminar-flow approach has been used for the microfabrication of engineered inorganic structures,<sup>[8a,b]</sup> patterned delivery of cells,<sup>[8c]</sup> manipulation with lipid bilayers,<sup>[9]</sup> separation and detection,<sup>[10,11]</sup> and in the adsorption of protein microstrips.<sup>[12]</sup> This approach is especially useful in handling proteins, cells, and other delicate biological structures, and it allows control of the spatial delivery of reagents inside microchannels.

In this work, we developed a microfluidic approach for the complex formation of polyelectrolyte and polyelectrolyte/protein microstrips on a glass surface. We also demonstrate experimentally a new, soft micropatterning technique for the anisotropic modification of micrometer-sized objects such as spherical microparticles and polyelectrolyte capsules. Synthesis of poly(dimethyldiallylammonium chloride)/poly(styrene sulfonate) (PDMA/PSS) and poly(dimethyldiallylammonium chloride)/bovine serum albumin (PDMA/BSA) microstrips is demonstrated with a laminar-flow microfluidic reactor. Resulting micropatterns are 8–10  $\mu\text{m}$  wide, separated by a gap of a few micrometers. The width of these microstrips, as well as their position in the microchannel, can be controlled by varying the flow rate and concentration of the individual components.

The synthetic procedure is schematically illustrated in Figure 1. Y- and S-type microchannel reactors (Figs. 1a,b) were employed to realize the formation of inter-polyelectrolyte and polyelectrolyte/protein micropatterns. To fabricate polyelectrolyte microarrays on a glass support, a poly(dimethylsiloxane) (PDMS) membrane with a pattern of channels molded into its surface was placed onto the flat surface of a glass slide (Fig. 1c). Each reactor channel was provided with two inlets and one outlet. Reagents from the inlet channels converge into a single laminar stream in the reactor microchannel. Each reagent solution was gently pumped into its inlet by a KdScientific pump. When two or more liquids flow in parallel at low Reynolds numbers ( $Re < 2000$ ), there is no turbulence

[\*] Prof. Y. M. Lvov, Dr. D. G. Shchukin, D. S. Kommireddy, Y. Zhao, Prof. T. Cui  
Institute for Micromanufacturing, LaTech  
Ruston, LA 71272 (USA)  
E-mail: ylvov@coes.latech.edu

Dr. G. B. Sukhorukov  
Max Planck Institute of Colloids and Interfaces  
1, Am Mühlenberg, D-14424 Potsdam (Germany)

[\*\*] We acknowledge financial support by the National Science Foundation grant NIRT-0210298, Louisiana BoR grant 02/05-RDA19, and from the Sofja Kovalevskaja Program of the Alexander von Humboldt Foundation. We thank A. Khalik and J. Palmer for help in model computations.